European Polymer Journal 44 (2008) 3482–3492

Contents lists available at ScienceDirect

European Polymer Journal

journal homepage: www.elsevier.com/locate/europolj

Macromolecular Nanotechnology

# Preparation, microstructure, and property characterizations of fluorinated polyimide–organosilicate hybrids

Tzu Hsuan Chiang [a], Szu-Ling Liu [b,1], Shyh-Yang Lee [b,2], Tsung-Eong Hsieh [b,*]

[a] Department of Environment Engineering, Chin Min Institute of Technology 110, Syuefu Road, Toufen Township, Miaoli County 351, Taiwan, ROC
[b] Department of Materials Science and Engineering, National Chiao Tung University 1001, Ta-Hsueh Road, Hsinchu 300, Taiwan, ROC

ARTICLE INFO

*Article history:*
Received 7 March 2008
Received in revised form 1 August 2008
Accepted 22 August 2008
Available online 30 August 2008

*Keywords:*
PI–organosilicate hybrids
Sol–gel process
Microstructure
Electrical properties

ABSTRACT

Synthesis of organosilicate (orgSi$O_2$) via sol-gel process utilizing tetraethoxysilane (TEOS) and diethoxydimethylsilane (DEDMS) as precursors was carried out in this work. Various amounts of orgSi$O_2$ were blended with fluorinated poly(amic acid) (PAA) to form the PAA–orgSi$O_2$ precursors and the fluorinated polyimide (PI)–orgSi$O_2$ (i.e., the HR1) thin-film hybrids were prepared via spin coating and curing treatments. The PI–orgSi$O_2$–AP (i.e., the HR2) hybrids were also prepared by using the PAA–orgSi$O_2$ precursors containing the amine silane coupling agent, the 3-aminopropyltriethoxysilane (APTEOS). The effects of APTEOS on promoting the crosslinking between organic and inorganic components as well as the network formation were investigated. Fourier-transform infrared spectroscopy (FTIR) showed that the orgSi$O_2$ particles indeed formed in the hybrids due to the emergence of absorption bands corresponding to Si—O—Si and O—Si—O bonds. Nuclear magnetic resonance (NMR) analyses revealed that the $Q^4$ units or, the four bridging bond units, dominate the structure of orgSi$O_2$. Thermal analysis indicated that the implantation of orgSi$O_2$ in PI matrix may effectively improve the thermal stability of hybrids. Transmission electron microscopy (TEM) revealed the formation of nano-scale orgSi$O_2$ particles in both hybrids and the sizes of orgSi$O_2$ are relating to the Si content. In HR1 hybrids, the particles obviously coarsened when Si content was high while, in HR2 hybrids, the addition of APTEOS effectively suppressed the phase separation and the ultrafine orgSi$O_2$ particles as small as 5 nm could be achieved in the sample with high Si content. Dielectric measurements showed that the lowest values of dielectric constants are 2.40 and 2.20 for HR1 hybrid at intermediate Si content = 0.4 mol and HR2 hybrid with the highest Si content = 0.8 mol, respectively. The suppression of dielectric constants was attributed to the absence of polar Si—OH and Si—$H_2O$ functional groups as well as the completion of hydrolysis in the hybrids. Formation of silica xerogels in the hybrids should be another cause of dielectric constant decrement, as indicated by the porosity calculation. Experimental results implied that the control of orgSi$O_2$ size to imply the closed-form silica structure is essential to the low-dielectric constant properties of hybrids. Leakage current density measurement illustrated that no deterioration effect occurs due to the addition of orgSi$O_2$ nanoparticles in polymeric matrix and satisfactory electrical properties are preserved for the hybrids for advanced low-dielectric applications.

© 2008 Elsevier Ltd. All rights reserved.

## 1. Introduction

As the feature sizes of integrated circuits (ICs) are scaled-down, interlayer dielectrics (ILDs) with low-dielectric constants are required in order to reduce the RC time

* Corresponding author. Tel.: +886 3 5712121x55306; fax: +886 3 5724727.
*E-mail address:* tehsieh@mail.nctu.edu.tw (T.-E. Hsieh).
[1] Current address: Taiwan Semiconductor Manufacturing Company (TSMC), Ltd., Taiwan, ROC.
[2] Current address: Golden View Technology Company, Ltd., Taiwan, ROC.

0014-3057/$ - see front matter © 2008 Elsevier Ltd. All rights reserved.
doi:10.1016/j.eurpolymj.2008.08.028

delay of integrated circuits (ICs) [1]. The ILDs can be either inorganic or organic types. Various inorganic ILDs with relative dielectric constants ($k$) as low as 2.0 have been developed [2], however, most of them are porous silica which suffers from the deficiencies such as inferior mechanical strength, high moisture absorption and high leakage current density. Alternatively, organic ILDs for sub-micro ICs are proposed and polyimides (PIs) are one of the promising types due to their high thermal stability and chemical resistance, low-dielectric constant (~3.5), good planarization capability and mechanical properties. As a matter of fact, PIs have been widely used in microelectronics, aerospace and other industrial applications [3]. For instance, PI is one of the important ILDs for advanced printed circuit boards (PCBs) and multichip module (MCM) packaging [4]. Nevertheless, PIs exhibit relatively high water absorption and large coefficient of thermal expansion (CTE) at about 56 ppm/°C, which limited their applications in the field of IC fabrication [5]. A common way to remedy such deficiencies is to form the organic–inorganic hybrids by incorporating reinforced inorganic fillers. Many efforts have been made to promote the phase compatibility in PI–silica hybrids [3,4] and the methods such as the introduction of the ethoxysilyl group into the polymer main chain [5] and blending of proper coupling agents in the precursor solution [6] have been proposed. Further, recent studies relating to the PI–silica composites containing nano-scale silica particles via the Sol–gel process reported that the measured densities of samples are lower than the theoretical values [7], implying the formation of porous structures in the hybrids. Kim et al. prepared the PI–silica hybrids by Sol–gel reaction of BPDA–PDA and tetraethoxsilane (TEOS) in acidic solution [8]. They found that the dielectric constant of the thin-film sample increases along with the increase of TEOS content. On the other hand, the dielectric constants of PI–silica hybrids could be effectively suppressed when 150 nm aerogels [9] or poly(silsesquioxane) (PSSQ) [10] was added in the hybrids. Kioul and Mascia utilized TEOS and diethoxydimethylsilane (DEDMS) as the porous crosslinked network former and modifier, respectively, to prepare the PI–silica hybrids [11]. Van Bommel et al. [12] found that a considerably fast Sol–gel reactions in the organically modified gels (i.e. DEDMS, phenyltriethoxysilane, methyltriethoxysilane) in comparison with non-modified TEOS.

Fluorinated PI possesses a lower dielectric constant in comparison with those of pristine PIs. This work prepares the fluorinated PI hybrids containing the organosilicate (orgSiO$_2$) particles via the Sol–gel reaction utilizing TEOS and DEDMS as the precursors. Furthermore, aminoalkoxysilane is one of the most widely adopted silane coupling agents for the modification of various oxide surfaces [13]. Another type of hybrids containing 3-aminopropyltriethoxysilane (APTEOS) was hence prepared and its effects on the improvement of affinity of silica phase with the polymeric matrix were investigated. This work studies the effects of Si contents and APTEOS addition on the microstructures of fluorinated PI–orgSiO$_2$ hybrids and evaluates the relationships with the hybrids' thermal/electrical properties. A viable way to prepare the thin-film hybrids with high thermal stability, low-dielectric constant and low leakage current density properties is demonstrated.

## 2. Experimental

### 2.1. Materials

Reagent grade chemicals were purchased for sample preparation. For the preparation of fluorinated PI, 4,4'-dia minodiphenylether (ODA) was from Merck-Schuehardt Co., *n,n*-dimethylacetamide (DMAc) and APTEOS were from ACROS Co., 2,2-bis(3,4-dicarboxyphenyl) hexafluoropropane dianhydride (6FDA) was from CHRISKEV., and ammonium hydroxide ($NH_4OH$) was from WAKO PURE Chemicals Industries, Ltd. Those chemicals are all with 99% purity. For the preparation of orgSiO$_2$, TEOS with 98% purity was supplied by TEDIA Co. and DEDMS with 99% purity was provided by Lancaster Co.

### 2.2. Preparation of fluorinated PAA and PAA–AP precursors

The fluorinated poly(amic acid) (PAA) precursor was prepared by first dissolving ODA in DMAc in nitrogen atmosphere. After soaking in an ice bath for 10 min, 6FDA was slowly added into the mixture at the molar ratios of 6FDA:ODA = 1:1. As to the PAA containing APTEOS (i.e., the PAA–AP precursor), the PAA with the molar ratio of 6FDA:ODA = 0.98:1 was first prepared and 0.02 mol of APTEOS were subsequently added. After the removal of ice bath, both mixtures were left along at room temperature and continuously stirred for 8 h to yield the PAA and PAA–AP precursor solutions with the solid contents = 20 wt%, respectively. The reaction schemes of PAA and PAA–AP precursors are depicted in Fig. 1.

### 2.3. Preparation of PI–orgSiO$_2$ and PI–orgSiO$_2$–AP thin-film hybrids

The orgSiO$_2$ precursors were prepared in weak base solution via Sol–gel process. The hydrolysis–condensation reaction of orgSiO$_2$ precursors for various types of hybrids was carried out at the conditions of $R = 0.5$ ($R$ = the molar ratio of water versus the molar ratio of organic functional groups of TEOS and DEDMS for hydrolysis) and TEOS:DEDMS:$H_2O$:EtOH:$NH_4OH$ (in molar ratio) = 1:0.5:2.5:20:0.5. The molar numbers of above ingredients for the preparation of orgSiO$_2$ precursors are listed in Table 1 in detail and in this work the sum of mole numbers of TEOS and DEDMS is defined as the theoretical Si content of hybrid sample.

After the complete mixing of above ingredients at room temperature for 6 h, the orgSiO$_2$ precursors were blended with PAA and PAA–AP precursors, respectively, and further stirred for 6 h at room temperature in nitrogen atmosphere to complete the preparation of PAA–orgSiO$_2$ and PAA–orgSiO$_2$–AP precursors. Afterward, the precursors were spin-coated on appropriate substrates and converted to the fluorinated PI–orgSiO$_2$ (termed as HR1 hereafter) and PI–orgSiO$_2$–AP (termed as HR2 hereafter) hybrid thin films via the curing process depicted in Fig. 2.

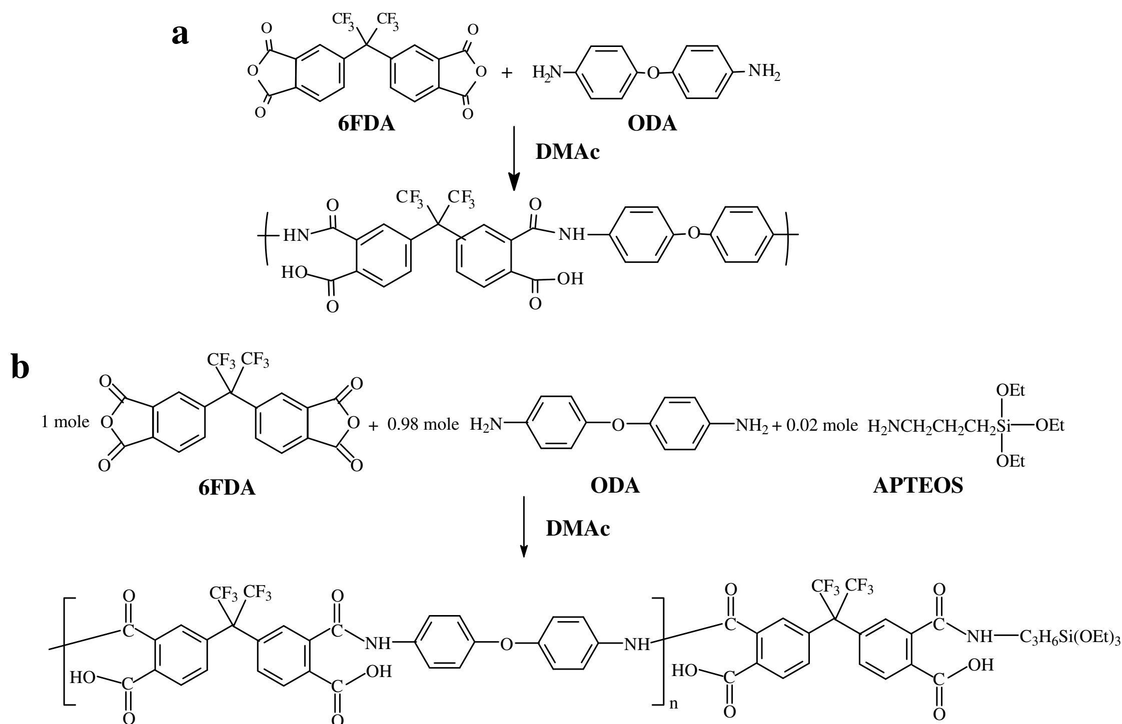


**Fig. 1.** Reaction schemes of (a) PAA and (b) PAA–AP precursors.

**Table 1**
A list of molar numbers of ingredients for the preparation of $orgSiO_2$ precursors for various hybrid samples

| Precursors[a] | Sample[b] | Theoretical Si content[c] (mol) | TEOS (mol) | DEDMS (mol) | $H_2O$ (mol) | EtOH (mol) | $NH_4OH$(mol) |
|---|---|---|---|---|---|---|---|
| PAA | HR1Si0.2 | 0.2 | 0.133 | 0.067 | 0.333 | 2.660 | 0.067 |
| | HR1Si0.3 | 0.3 | 0.200 | 0.100 | 0.500 | 4.000 | 0.100 |
| | HR1Si0.4 | 0.4 | 0.266 | 0.134 | 0.665 | 5.320 | 0.134 |
| | HR1Si0.5 | 0.5 | 0.333 | 0.167 | 0.833 | 6.667 | 0.167 |
| | HR1Si0.6 | 0.6 | 0.400 | 0.200 | 1.000 | 8.000 | 0.200 |
| | HR1Si0.8 | 0.8 | 0.532 | 0.268 | 1.330 | 10.640 | 0.268 |
| PAA–AP | HR2Si0.4 | 0.4 | 0.266 | 0.134 | 0.665 | 5.320 | 0.134 |
| | HR2Si0.5 | 0.5 | 0.333 | 0.167 | 0.833 | 6.667 | 0.167 |
| | HR2Si0.6 | 0.6 | 0.400 | 0.200 | 1.000 | 8.000 | 0.200 |
| | HR2Si0.8 | 0.8 | 0.532 | 0.268 | 1.330 | 10.640 | 0.268 |

[a] Initially, 2 mol of PAA or PAA–AP was prepared, then added above ingredients to form the PAA–$orgSiO_2$ and PAA–$orgSiO_2$–AP precursors.
[b] The samples are denoted by HR*X*Si*Y* in which *X* represents the hybrid type (*X* = 1 or 2) while *Y* represents the theoretical Si content in mol (*Y* = 0.2–0.8).
[c] The sum of mole numbers of TEOS and DEDMS is defined as the theoretical Si content of hybrid sample.

In below, the symbols for hybrid samples are designated as HR*X*Si*Y* in which *X* represents the hybrid type (*X* = 1 or 2) while *Y* represents the theoretical Si content (*Y* = 0.2–0.8, in the unit of mole).

### 2.4. Infrared spectroscopy

The samples for Fourier-transform infrared spectroscopy (FTIR) were prepared by spin coating the precursors on KBr discs. The FTIR measurements were performed on the samples subjected to soft baking at 90 °C for 10 min followed by the curing treatment with temperature profile shown in Fig. 2. The FTIR analyses were carried out in a Nicolet Protégé™-460 FTIR spectrometer in the wave number ranging from 400 to 4000 $cm^{-1}$. The data were collected with the resolution of 4 $cm^{-1}$ by spectral average at least 16 scans.

### 2.5. Solid-state $^{29}Si$ nuclear magnetic resonance spectroscopy ($^{29}Si$ NMR)

The preparation of hybrid samples for NMR analysis is similar to that for FTIR analysis. After the completion of curing, the thin-film hybrids were cut into small pieces about $5 \times 5$ $mm^2$ in size and 500 nm in thicknesses. They were then sent to a Bruker DSX400WB NMR to obtain the $^{29}Si$ NMR spectra. The analysis was carried out at room temperature with the sample spinning rate = 7 kHz.

### 2.6. Thermogravimetric analysis (TGA)

The 10% weight loss decomposition temperature ($T_d$) was measured by using a thermogravimetric analyzer (Du Pont Instruments TGA 2950) from room temperature to 900 °C

MACROMOLECULAR NANOTECHNOLOGY

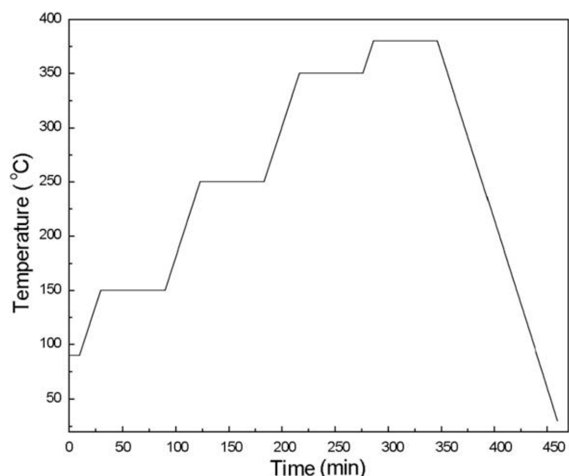


**Fig. 2.** Temperature profile of curing process for hybrid samples.

at a heating rate of 10 °C/min in nitrogen atmosphere. The TGA analysis was also carried out in air atmosphere so as to obtain the residual weight of inorganic content.

### 2.7. Transmission electron microscopy (TEM)

The preparation of hybrid samples for TEM characterization is similar to that for FTIR analysis as described in Section 2.4. After dissolving the KBr away in DI water, the hybrid layer was mounted on the Cu mesh and then transferred to a JEOL 2000FX TEM for microstructure characterization. The TEM, with a $LaB_6$ electron source, was operating at 200 kV and all micrographs were taken at bright-field image mode.

### 2.8. Electrical property measurements

In this work, the metal–insulator–metal (MIM) samples were elaborated for electrical measurements. First, bottom electrode comprised of the sequential layer of 20-nm thick Ti and 150-nm thick Pt were deposited on oxidized Si wafer by sputtering process. In bottom electrode, the Ti layer serves as the adhesive layer on Si substrate while Pt, the noble metal layer with good resistance to oxidation, is to provide sufficient adhesion for subsequent hybrid layer to ensure successful sample preparation. About 500-nm thick fluorinated PI–$orgSiO_2$ hybrid layer was then formed on the top of bottom electrode via the spin-coating and curing steps described previously. Afterward, a $4 \times 5$ array of circular Al top electrodes with various diameters (2, 4, 6 and 8 mm) were deposited on the cured hybrid layer by sputtering to complete the MIM sample preparation. Aluminum, the inexpensive and most commonly adopted electrode metal, was simply chosen to serve as the conducting agent for electrical probing during measurements.

The dielectric constants of hybrid samples were measured by using a HP 4280A capacitance meter at fixed frequency of 1 MHz. The current–voltage ($I$–$V$) characteristics of the samples were obtained by a HP 4156B semiconductor parameter analyzer at the applied bias ranging from 0 to 1.6 MV/cm. Electrical measurements were carried out in a shielded probe station (Model S-1007x-6, SIGNATONE, USA) at room temperature under 40–50% RH. The test fixture containing tungsten probes with 10-μm tip radius was adopted to achieve the electrical contact on the electrodes of samples. For each type of hybrid sample, five sets of MIM samples were prepared. By ignoring the highest and lowest values obtained during the measurements, the average values of the measured data were calculated and presented as the electrical properties of hybrids.

## 3. Results and discussion

### 3.1. FTIR analysis

FTIR analysis indicated that the two types of hybrids exhibit similar spectra in regard of the formation of org-$SiO_2$ in the samples. To avoid the redundancy, only the FTIR spectra of HR2 hybrids are presented as follows. Fig. 3 presents the FTIR spectra of HR2 hybrids with various theoretical Si contents subjected to soft baking treatment. Formation of $orgSiO_2$ is deduced by the absorption bands appearing at around 804 $cm^{-1}$ for Si—O—Si symmetric stretching vibrations and at 465 $cm^{-1}$ for O—Si—O vibration as shown in Fig. 3. These evidence the occurrence of hydrolysis reaction of TEOS and DEDMS [14]. Fig. 3 also shows that the intensity heights corresponding to Si—O—Si and O—Si—O peaks increase with the increase of Si content, illustrating more $orgSiO_2$ forms in the sample when Si content is increased. Furthermore, the peak at 1656 $cm^{-1}$ corresponding to C=O of amides and the peak 1543.5 $cm^{-1}$ corresponding to combination absorbance of N—H and C—N of amides emerges for the hybrid samples prior to curing. However, such characteristic peaks diminish in the cured hybrid sample as shown in Fig. 4. The occurrence

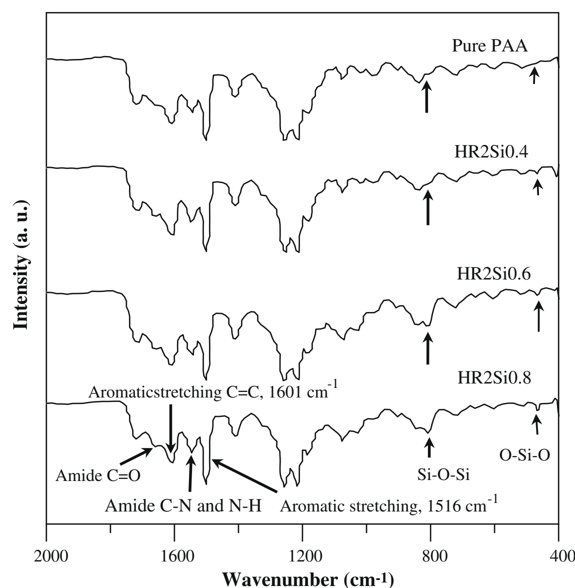


**Fig. 3.** FTIR spectra of HR2 hybrids containing various theoretical Si contents subjected to soft baking treatment.

MACROMOLECULAR NANOTECHNOLOGY

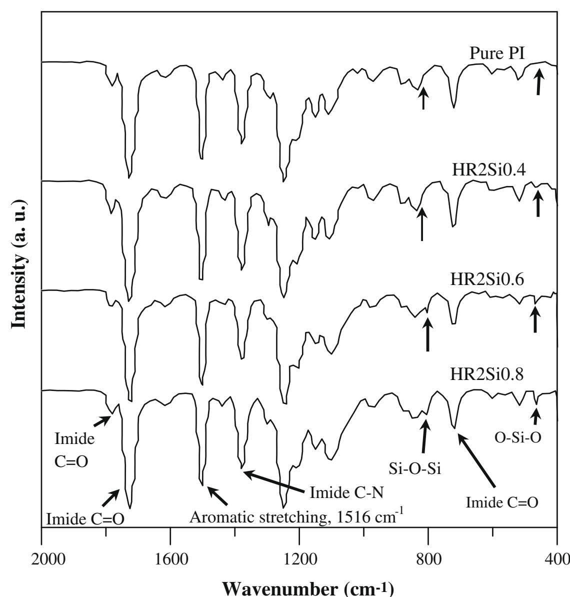


**Fig. 4.** FTIR spectra of HR2 hybrids containing various theoretical Si contents subjected to curing process shown in Fig. 1.

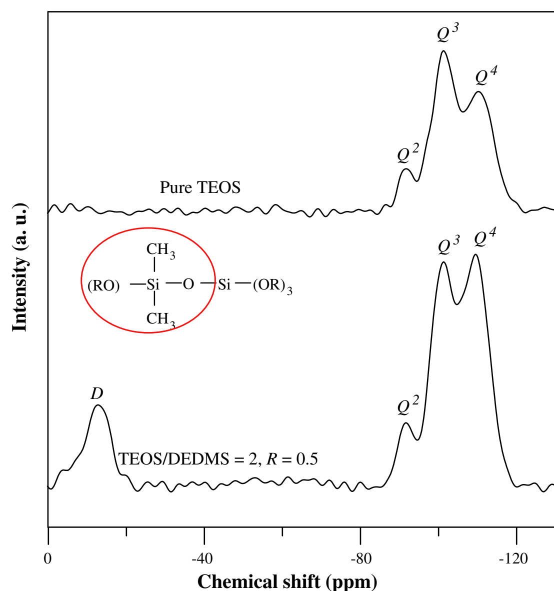


**Fig. 5.** $^{29}$Si NMR spectra of organosilicates derived from TEOS and TEOS/DEDMS = 2 at $R = 0.5$.

of imidization in the cured hybrid samples is also evidenced by the simultaneous emergence of the 1781 $cm^{-1}$ peak corresponding to asymmetric stretching C=O of imide, the 1720 $cm^{-1}$ peak corresponding to symmetric C=O stretching of imide, the 1380 $cm^{-1}$ peak corresponding to C-N stretching of imide and the 725 $cm^{-1}$ peak corresponding to C=O bending of imide [15]. Finally, we note that the peaks at 804 $cm^{-1}$ corresponding to the Si—O—Si network vibrations are present in all FTIR spectra of cured hybrid samples.

### 3.2. $^{29}$Si NMR analysis

Fig. 5 presents the $^{29}$Si NMR spectra of orgSiO$_2$ derived from pure TEOS and TEOS/DEDMS via the Sol–gel reaction. In both cases, the peaks at −110, −100 to −104 and −90 ppm respectively corresponding to the structural units $Si(O_{0.5})_4$ ($Q^4$, the four bridging bond unit), the $(RO)Si(O_{0.5})_3$ ($Q^3$, the three bridging bond unit), and $(RO)Si(O_{0.5})_2$ ($Q^2$, the two bridging bond unit) are observed [16]. The presence of $Q^2$ and $Q^3$ peaks indicates the incomplete hydrolysis resulted from the uncondensed silanol in orgSiO$_2$. For TEOS/DEDMS (mole ratio = 2, $R = 0.5$), an extra peak at −12.61 ppm appears. It implies the presence of $-(CH_3)_2SiO-$ functional group (i.e., the *D* unit) in orgSiO$_2$ [17] due to the addition of DEDMS. Furthermore, the intensity of peak corresponding to $Q^4$ unit at −110 ppm is obviously higher for the case of TEOS/DEDMS, indicating a more complete hydrolysis in comparison with pure TEOS [18].

Fig. 6 presents the $^{29}$Si NMR spectra for the cured HR1 and HR2 hybrids. It can be seen that the curing treatment implies the dominance of $Q^4$ units in orgSiO$_2$ structure for both hybrid samples. A negligibly small amount of $Q^3$ units remains in HR1 hybrids, indicating the existence of few uncondensed silanol in such hybrids. Further, the peaks at about −18 to 21 ppm imply the presence of *D* units in both hybrids. In comparison with the $^{29}$Si NMR spectra of orgSiO$_2$ shown in Fig. 5, there are obvious peak shifts for *D* units in the hybrid samples. This is attributed to the strong hydrogen bonds in the interpenetrating network (IPN) structure formed by the intercalation of PI and Si—O—Si structure during polymerization [7,9].

### 3.3. Thermal properties

Table 2 summarizes the results of TGA analysis for HR1 and HR2 hybrid samples with various Si contents. It can be

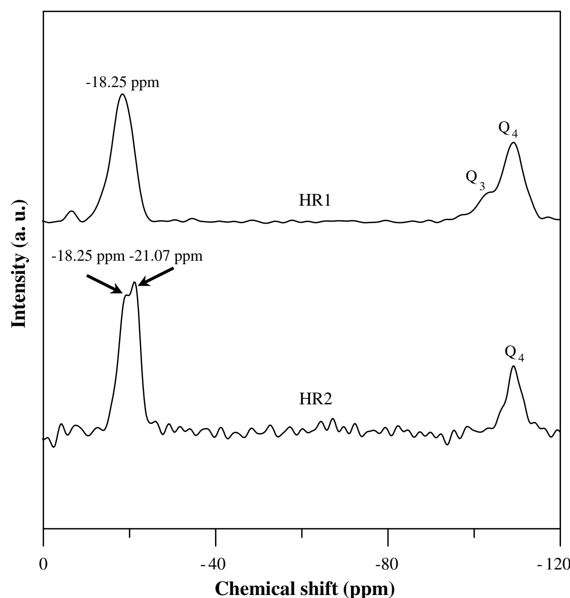


**Fig. 6.** $^{29}$Si NMR spectra of HR1 and HR2 samples.

**Table 2**
Analytical results of TGA on HR1 and HR2 hybrids

| Sample[a] | Theoretical Si content (wt%) | $T_d$ (°C) | | $R_c$ (wt%) |
|---|---|---|---|---|
| | | in $N_2$ | in air | |
| PI | 0 | 567 | 561 | 0.11 |
| HR1Si0.2 | 2.41 | 565 | 556 | 0.15 |
| HR1Si0.3 | 4.05 | 574 | 563 | 0.29 |
| HR1Si0.4 | 6.17 | 581 | 566 | 0.39 |
| HR1Si0.5 | 8.98 | 582 | 565 | 0.43 |
| HR1Si0.6 | 12.89 | 588 | 568 | 0.90 |
| HR1Si0.8 | 28.27 | 592 | 569 | 1.76 |
| HR2Si0.4 | 6.17 | 584 | 563 | 0.29 |
| HR2Si0.5 | 8.98 | 589 | 569 | 0.31 |
| HR2Si0.6 | 12.89 | 591 | 576 | 1.22 |
| HR2Si0.8 | 28.29 | 594 | 571 | 2.46 |

[a] Hybrid samples are denoted by HR*X*Si*Y* in which *X* represents the hybrid type (*X* = 1 or 2) while *Y* represents the theoretical Si content in mol (*Y* = 0.2–0.8).

seen that regardless of the test atmosphere type, the $T_d$'s of hybrids increase with the increase of Si content. This implies that the increment of $orgSiO_2$ benefits the thermal stability of hybrids, a result similar to previous studies, e.g., phenolic/silica nanocomposites [19]. We note that all hybrids exhibit inferior thermal stability in air atmosphere, indicating that the organo groups of $orgSiO_2$ are less stable in oxygen environment. As listed in Table 2, the residual weight percentages ($R_c$'s) of hybrids increase with the increase of theoretical Si content. The hybrids prepared at high Si contents display a high char yield due to the high amount of $orgSiO_2$ formed in the samples [9]. Furthermore, the values of $R_c$'s of HR2 samples become higher than those of HR1 samples when theoretical Si content >0.6 mol. This is ascribed to the addition of APTEOS which is commonly known as an inorganic crosslinking agent. It has been reported that the amino group on APTEOS affects the crosslinking reactions in copolymer containing anhydride [20]. The anhydride group of 6FDA on PAA–AP precursors reacts with the amino group on APTEOS via the reaction shown in Fig. 7. When the unshared electron pair on amino group is delocalized by interacting with the anhydride group, it simultaneously enhances the crosslinking with silanol groups on APTEOS and hence promotes the network formation in $orgSiO_2$ resulted from the Sol–gel reaction of TEOS/DEMOS [21,22].

### 3.4. TEM microstructure characterizations

Figs. 8 and 9 present the TEM micrographs of HR1 and HR2 hybrid samples with various Si contents, respectively. In HR1 samples, $orgSiO_2$ particles with the size $\leqslant$10 nm are observed when Si content $\leqslant$0.4 mol, whereas apparent particle coarsening occurs in the samples with high Si content, e.g., HR1Si0.8. Fig. 9(a) revealed that the $orgSiO_2$ particles can barely observed in the HR2 samples with Si content = 0.4 mol. In HR2Si0.8 sample, the $orgSiO_2$ particles are as small as 5 nm as shown in Fig. 9(c). It is apparent that, at the same Si content, the $orgSiO_2$ particles in HR2 samples are much smaller than those in HR1 samples. The fine dispersion of $orgSiO_2$ particles in PI matrix is caused by two factors: (1) the chain interactions between PAA and TEOS or APTEOS (precursors of silica) decrease the tendency of silica aggregation during hydrolysis of alkoxide groups (i.e., formation of silica) [23]; (2) the high rigidity of PI chains prevents the aggregation of $orgSiO_2$ particles at the imidization stage [24]. TEM characterization clearly illustrated that the addition of APTEOS dramatically suppresses the phase separation in HR2 hybrids due to the enhancement of connection between the end group of PI and the triethoxysilane group of $orgSiO_2$ [9]. The amino group in APTEOS is known to suppress the hydrophilicity of hybrid [21]. It effectively modifies the surface of inorganic phase and increases the conjugation between $orgSiO_2$ particles [25]. Suppression of phase separation thus implies less aggregation and hence ultra small $orgSiO_2$ particles in HR2 hybrids.

### 3.5. Dielectric constant properties of thin–film hybrids

Dielectric constant of dense silica ($k$ = 4.0) [26] is higher than that of fluorinated PI ($k$ = 2.88). Therefore, as predicted by dielectric model of composites [23], the addition of silica in PI should raise the dielectric constant of hybrid [8]. Nevertheless, distinct behaviors of dielectric constants for the hybrids were observed in this work. As shown in Table 3, the dielectric constant of HR1 hybrid decreases

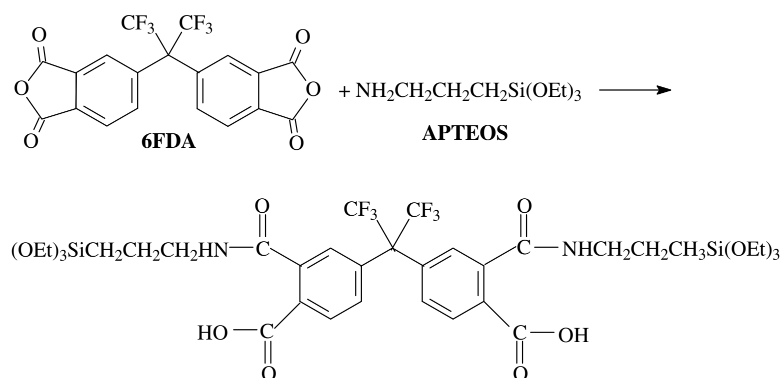


**Fig. 7.** Reaction of APTEOS with 6FDA on PAA–AP precursors.

MACROMOLECULAR NANOTECHNOLOGY

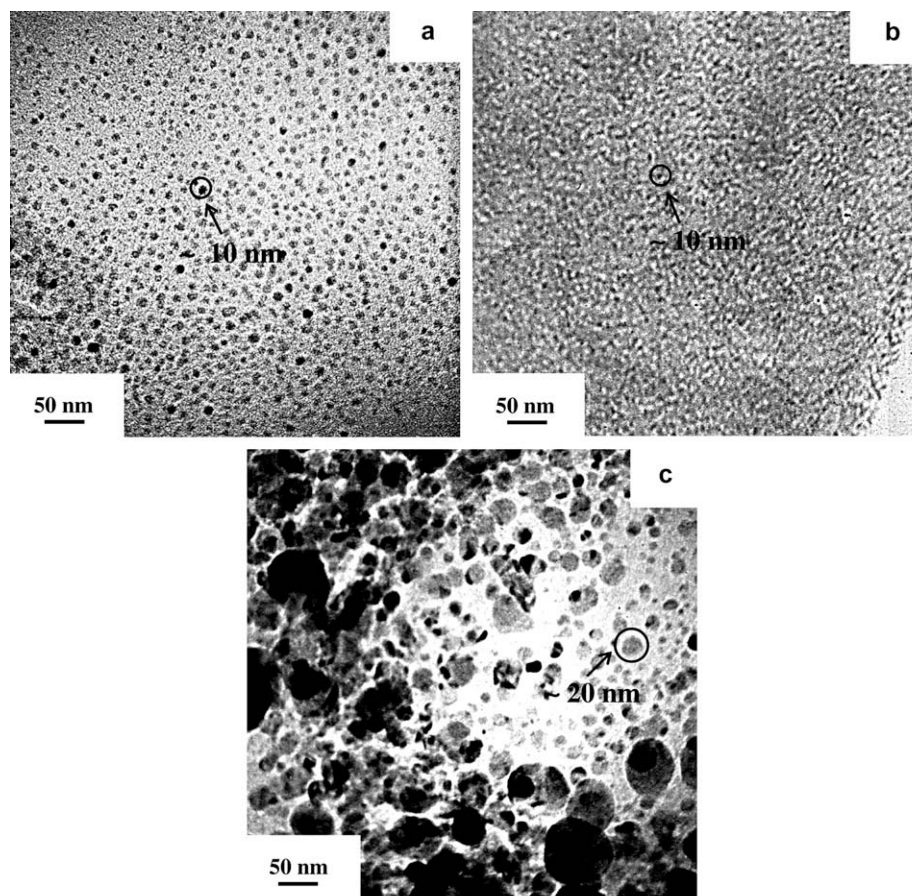


**Fig. 8.** Bright-field TEM micrographs of HR1 hybrids (PI–orgSiO$_2$): (a) HR1Si40; (b) HR1Si50; (c) HR1Si80. The images were taken by TEM operating at 200 kV.

with the increase of Si content, reaches a minimum value of 2.40 at about Si content = 0.4 mol, then increases with the Si content. As to the HR2 hybrids, the dielectric constant decreases monotonously with the increase of Si contents and the lowest dielectric constant about 2.20 is achieved in the HR2Si0.8 sample. The explanations of dielectric constant changes for these two types of hybrids are presented as follows.

FTIR analysis revealed that there is no Si—OH and Si—$H_2O$ stretching vibrations at 3450, 950 and 1635 cm$^{-1}$ for both types of hybrids as shown in Fig. 4. Absence of polar Si—OH and Si—$H_2O$ functional groups and the completion of hydrolysis hence imply the dielectric constant decrement of hybrid samples. As mentioned above, the amino group on APTEOS tends to decrease the hydrophilicity of HR2 hybrid [21]. In conjunction with the fine orgSiO$_2$ particle size and large specific surface area, the suppression of hydrophilicity in HR2 hybrids effectively limits the motions of polar functional groups presented at the PI/orgSiO$_2$ interfaces. Thus, the low-dielectric constant property was obtained.

As shown in Fig. 6, the NMR analysis indicated that the $Q^4$ units dominate the orgSiO$_2$ structure in both hybrids. The dominance of such a four bridging bond units implies that the silica are built up in three-dimensional manner and, hence, it is speculated that the formation of porous silica, i.e., silica aerogel or xerogel [27], might play an important role in the suppression of dielectric constants of hybrids as listed in Table 3. Aerogel and xerogel are the terms commonly adopted to depict the porous silica containing various amounts of nano-scale pores. They may be classified in terms of the porosity inside, e.g., for aerogels, porosity >75%; for xerogels, porosity <75%; for dense hybrids, porosity <1% [28].

In terms of the measured values of $k$, we calculated the densities ($\rho_1$ and $\rho_2$) and porosities ($\Pi_1$ and $\Pi_2$) for the cases of silica xerogel and aerogel by utilizing the following expressions [28,29]:

$$k = 1 + 1.28\rho_1 \quad (1)$$

$$k = 1 + 1.6\rho_2 \quad (2)$$

$$\Pi = 1 - \frac{\rho}{\rho_s} \quad (3)$$

where $\rho_s = 2.27$ g/cm$^3$ for silica xerogel [28] and $\rho_s = 2.19$ g/cm$^3$ for silica aerogel were adopted for Eq. (3) [30]. Table 3 lists the calculated results. All the values of

MACROMOLECULAR NANOTECHNOLOGY

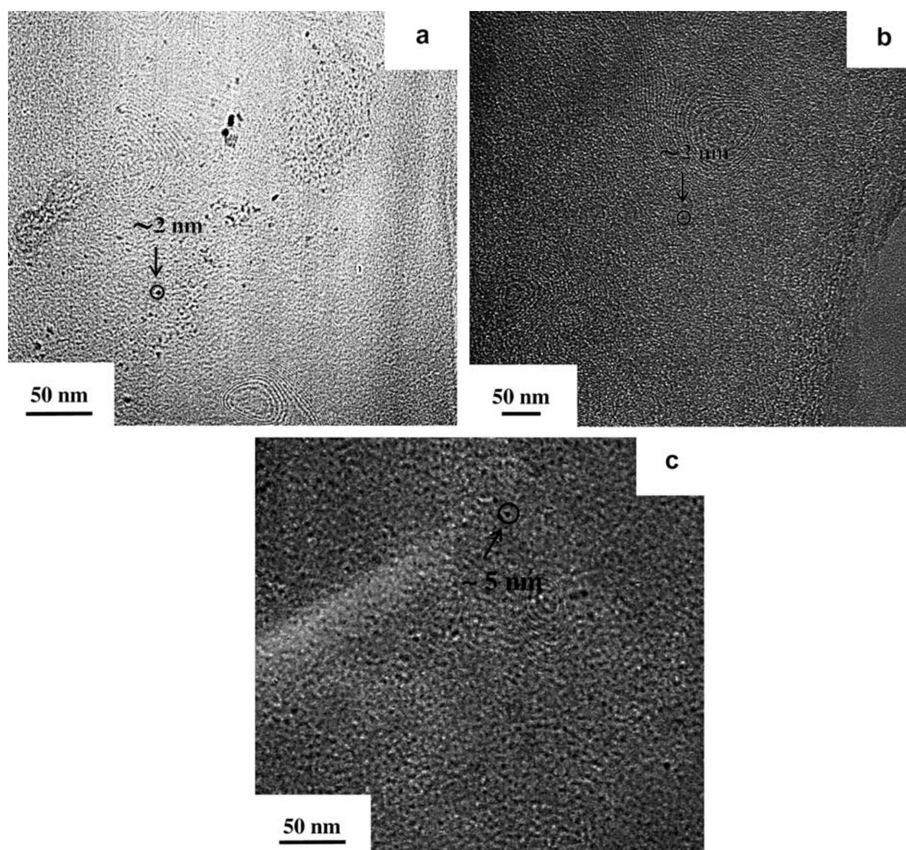


**Fig. 9.** Bright-field TEM micrographs of HR2 hybrids (PI–orgSiO$_2$–AP): (a) HR2Si40; (b) HR2Si50; (c) HR2Si80. The images were taken by TEM operating at 200 kV.

porosity are <75%, implying the formation of silica xerogels in both hybrids. The content of silica xerogel increases with the Si content which, in turn, results in the decrease of dielectric constants of hybrids. Nevertheless, the dielectric constants of HR1 hybrids gradually deteriorate when the theoretical Si contents exceed 0.5 mol. This is ascribed to the coarsening of orgSiO$_2$ particles as revealed by TEM characterization shown in Fig. 8(c). Since coarsening is commonly driven by the reduction of total surface energy of system, it might diminish the porosity in the hybrids and hence deteriorate their dielectric properties.

A distinct feature revealed by the TEM characterizations and dielectric measurements presented above is that the lowest dielectric constants indeed occur in the hybrids with specific orgSiO$_2$ particle sizes. For HR1 hybrids, it occurs in the samples with intermediate Si contents; for instance, the lowest dielectric constant of 2.40 is achieved in HR1Si0.4 in which the size of orgSiO$_2$ is about 5 nm. As to the HR2 hybrids, previous TEM characterizations revealed that the addition of APTEOS causes the refinement of orgSiO$_2$ particles and results in an ultra-small, uniform distribution of silica in the samples. Ultrafine orgSiO$_2$ with high porosity seems to imply the low-dielectric constant property; nevertheless, the effectiveness to suppress the dielectric constant becomes obvious in HR2 sample with the highest Si content, e.g., the HR2Si0.8 hybrid with orgSiO$_2$ about 5 nm in size. As shown by Figs. 9(a) and (b), the orgSiO$_2$ particles are as small as 2 nm in HR2 hybrids with small or intermediate Si contents. Lack of distinct image contrast of orgSiO$_2$ particles in Figs. 9(a) and

**Table 3**
Dielectric constant, calculated densities and porosities of hybrid samples with various theoretical Si contents

| Sample[a] | $k$ | $\rho_1$[b] (g/cm$^3$) | $\rho_2$[c] (g/cm$^3$) | Porosity[b] $\Pi_1$ (%) | Porosity[c] $\Pi_2$ (%) |
|---|---|---|---|---|---|
| PI | 2.87 | – | – | – | – |
| HR1Si0.2 | 2.64 | 1.28 | 1.03 | 43.6 | 53.20 |
| HR1Si0.3 | 2.56 | 1.22 | 0.98 | 46.4 | 55.48 |
| HR1Si0.4 | 2.40 | 1.09 | 0.88 | 51.8 | 60.05 |
| HR1Si0.5 | 2.43 | 1.12 | 0.89 | 50.7 | 59.19 |
| HR1Si0.6 | 2.49 | 1.16 | 0.93 | 48.8 | 57.48 |
| HR1Si0.8 | 2.51 | 1.18 | 0.94 | 48.2 | 56.91 |
| HR2Si0.4 | 2.66 | 1.30 | 1.04 | 42.9 | 52.6 |
| HR2Si0.5 | 2.60 | 1.25 | 1.00 | 44.9 | 54.3 |
| HR2Si0.6 | 2.53 | 1.20 | 0.96 | 47.3 | 56.3 |
| HR2Si0.8 | 2.20 | 0.94 | 0.75 | 58.7 | 65.8 |

[a] Hybrid samples are denoted by HR*X*Si*Y* in which *X* represents the hybrid type (*X* = 1 or 2) while *Y* represents the theoretical Si content in mol (*Y* = 0.4–0.8).
[b] For xerogel, $k = 1 + 1.28\rho_1$; $k$ is dielectric constant; $\rho_1$ is density; $\Pi_1$ is porosity.
[c] For aerogel, $k = 1 + 1.6\rho_2$; $k$ is dielectric constant; $\rho_2$ is density; $\Pi_2$ is porosity.

(b) indicates that in such samples the org$SiO_2$ particles are likely in open form that the polymeric component might invade the pore space in org$SiO_2$ and, thus, diminish its effects on suppressing the dielectric constant. It is believed that, with the growth of particle size, the org$SiO_2$ structure is prone to be the closed form and thus the porosity effects become obvious on the reduction of dielectric constant of hybrids. The results above hence illustrate that the growth control of inorganic filler to form the closed-form structure is the key issue to achieve satisfactory dielectric properties in the hybrids containing porous silica particles.

The HR2 hybrids were also aged in a room-temperature atmosphere with 85% relative humidity to evaluate the effects of moisture absorption on dielectric constants of hybrids. As show in Fig. 10, the dielectric constants of hybrids increase with the aging time regardless of the amounts of Si contents. However, the dielectric constants increase only in first few days of aging and then insignificantly increase with further increase of aging time. The deterioration of dielectric constants is attributed to the residual silanol groups and/or the moisture absorption in the hybrids. Fig. 10 also shows that the resistance to the deterioration of dielectric constant improves with the increase Si content in the hybrid. These results somehow reflect the pore morphology in the hybrids. When the pores are in closed form, the condensation of moisture inside the pores becomes difficult and hence satisfactory dielectric properties could be preserved in the hybrids with high Si contents [31].

### 3.6. Leakage current densities of thin-film hybrids

Fig. 11 presents the leakage current densities of hybrid samples versus the applied bias field up to 1.6 MV/cm. The absence of electrical breakdown shown in the figure indicates the fluorinated PI–org$SiO_2$ hybrids preserve satisfactory resistance property which is comparable to those for commercial PI products [32]. This illustrates that the addition of porous inorganic fillers does not dramatically escalate the charge carrier transport in polymeric matrix.

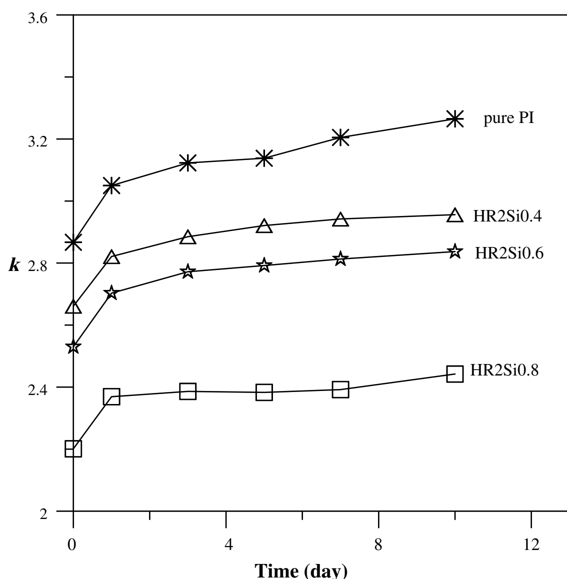


**Fig. 10.** The dielectric constant changes of HR2 hybrids as a function of aging time in a room-temperature atmosphere with 85% relative humidity.

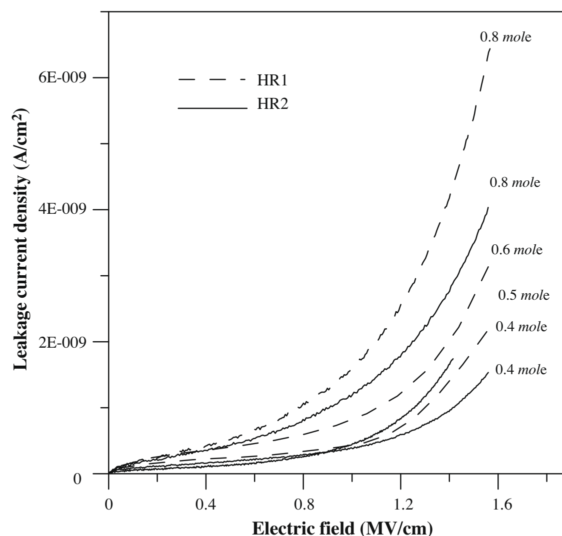


**Fig. 11.** Leakage current density versus applied bias field of HR1 and HR2 hybrids.

In contemporary IC process, various low-κ materials, organic types such as fluorinated polymers, parylene and bisbenzocyclobutene (BCB), hybrid types such as organosilicate glasses (OSG), hydrogen silsesquioxanes (HSQ) and methyl silsesquioxanes (MSQ), inorganic types such as fluorinated oxide (SiOF), porous silica and mesoporous silica films, have been proposed for ILD usages [33]. To fulfill such applications, leakage current property is an essential issue for device performance and processing considerations. At 1 MV/cm, fluorinated PI with leakage current = 1.8 pA [34], DuPont's PI 2610 with leakage current densities = $10^{-6}$ A/cm$^2$ [3] and BCB with leakage current densities = $10^{-8}$ A/cm$^2$ [35] were reported. At the same bias field, porous OSG, aromatic hydrocarbon polymer (i.e., SiLK), HSQ and MSQ respectively exhibit the leakage current densities about $10^{-9}$ A/cm$^2$ [36], $10^{-9}$ A/cm$^2$ [37], $10^{-8}$ A/cm$^2$ [38,39] and >$10^{-8}$ A/cm$^2$ [40]. Leakage current densities ranging from $10^{-6}$ to $10^{-7}$ A/cm$^2$ have been reported for SiOF films at 1 MV/cm [41,42]. A study of Sol–gel -derived mesoporous silica film indicated the leakage current density decreases from $8.4 \times 10^{-3}$ to $1.6 \times 10^{-7}$ A/cm$^2$ at 1 MV/cm when its annealed temperature increases from 300 to 450 °C [43]. Similarly, Al/xerogel showed the temperature-dependent leakage current densities in the range of $10^{-6}$–$10^{-9}$ A/cm$^2$ [44]. Fig. 11 depicts that, regardless of hybrid types prepared in this work, the leakage current densities are in the order of magnitude of $10^{-9}$ A/cm$^2$, which are at about the same level in comparison with those advanced low-κ materials. The relatively low leakage current property in conjunction with the low-dielectric constant property presented previously hence illustrate that the fluorinated PI–org$SiO_2$ hybrids may be an alternative for low-κ dielectric applications.

Fig. 11 shows that the leakage current density increases with the increase of Si content for both hybrids. This is ascribed to the increase of PI/orgSiO$_2$ interfaces and pore content in the samples derived in previous calculation. Interface is a typical planar defect where the disruption of chemical bonds occurs. The dangling bonds at such a structural discontinuity may thus serve as the paths for charge carrier transport. The leakage current density is hence increase with the Si contents in the hybrids due to the presence of more PI/orgSiO$_2$ interfaces. Yu et al. reported that there are more Si—C bonds with lonely electron pairs in thin film sample with high pore content [45]. This might similarly occur in our hybrid samples with high Si content and thereby result in the increase of leakage current density. Deterioration of electrical properties caused by the addition of inorganic filler was also reported by Lin et al. who studied the low-κ nanocomposite thin films comprised of silica nanoparticle and thermoset SiLK polymer [46]. They found the breakdown field and leakage current density respectively increase from 5 MV/cm and $<10^{-9}$ A/cm$^2$ for pristine SiLK film to 1 MV/cm and $>10^{-3}$ A/cm$^2$ for hybrid film containing 19.7 wt% of silica nanoparticles. The detrimental effect was ascribed to the impure silica nanoparticle solution used in their study. Though the increase of leakage current density with the increase of silica content was similar to that reported by Lin et al., no dramatic deterioration occurred in this work. On the contrary, the study on low-κ 3NH$_2$–silicates/6FDA–ODA nanocomposites showed the implantation of layered inorganic fillers suppresses the charge carrier transport in polymeric matrix [47]. This implies the morphology of inorganic fillers may also affect the electrical properties of low-κ materials.

Fig. 11 also shows that at the same Si content, the leakage current density of HR1 hybrid is higher than that of HR2 hybrid. Since there is no addition of APTEOS in HR1 hybrids to promote the crosslinking, they might contain residual hydroxyl groups after the condensation process. The hydroxyl groups would absorb the moisture in environment and thus increase the leakage current density of the hybrids. Besides, the improvement of affinity between organic and inorganic phases due to the addition of APTEOS is able to retard the charge carrier transport along the PI/orgSiO$_2$ interfaces. Lower leakage current property is hence obtained in HR2 hybrid in comparison with HR1 hybrid at the same Si content.

Finally, the low-κ dielectrics must possess sufficient mechanical properties to support the device integrity and endure the damages resulted from fabrication processes, e.g., the chemical mechanical polishing (CMP). Due to the lack of appropriate tools such as nanoindentation at hand, this work did not perform the mechanical property test for hybrid samples. However, the elastic modulus ($E$) of pristine 6FDA–ODA is found to be 2 GPa [47], which is comparable to those of popular low-κ materials (for PI, $E \approx 2$ GPa; for BCB, $E \approx 3$ GPa; for SiLK, $E \approx 2.5$ GPa; for MSQ, $E \approx 1$ to 2 GPa; for xerogel glycol, $E \approx$ 3–10 GPa) [33]. Previous studies on the low-κ nanocomposites simultaneously revealed the improvement of mechanical properties due to addition of inorganic fillers [46,47]. It is believed that via the formation of nanocomposite, the mechanical properties of fluorinated PI–orgSiO$_2$ hybrid films would be similarly improved to meet the application requirements of advanced low-κ ILDs.

## 4. Conclusions

This work prepares two types of fluorinated PI–orgSiO$_2$ hybrid thin-film samples, the PI–orgSiO$_2$ (termed as HR1) and the PI–orgSiO$_2$–AP (termed as HR2), utilizing TEOS/DEDMS as the precursor and investigates the relationships between microstructures and thermal/electrical properties. In HR2 hybrids, the amine silane coupling agent, APTEOS, was added so as to explore its effects on the modification of the affinity of TEOS with the PI matrix. The FTIR analysis revealed that the Sol–gel reaction of TEOS and DEDMS indeed occurs and the presence of absorption bands for Si—O—Si and O—Si—O bonds evidence the formation of orgSiO$_2$ particles in the hybrids. The $^{29}$Si NMR analysis illustrated the dominance of $Q^4$ units or, the four bridging bond unit, in the structure of orgSiO$_2$ as well as the presence of $D$ units (i.e., the —(CH$_3$)$_2$SiO— functional group) in the hybrids. The specific $D$ structural unit is resulted from the strong hydrogen bonds in the interpenetrating network (IPN) structure formed by the intercalation of PI and Si—O—Si structure during polymerization. TEM characterization revealed the presence of nano-scale orgSiO$_2$ particles in both hybrids and the orgSiO$_2$ particle size increases with the Si content. In HR1 hybrids, particle coarsening became obvious when Si content exceeded 0.5 mol. In HR2 hybrids, the sizes of orgSiO$_2$ particles as small as 5 nm were observed in the sample with the highest Si content of 0.8 mol. This evidenced that the addition of APTEOS may effectively promote the connection of the end group of PI with triethoxysilane group and thus suppresses the phase separation in the hybrids. Furthermore, the formation of orgSiO$_2$ particles was found to benefit the thermal stability of hybrids, as indicated by the thermal degradation temperatures ($T_d$'s) of hybrids obtained by TGA analysis.

Dielectric measurements found that the formation of orgSiO$_2$ particles suppresses the dielectric constants of hybrids. Dielectric constants as low as 2.40 and 2.20 were obtained for HR1 hybrid with intermediate Si content = 0.4 mol and HR2 hybrid with the highest Si content = 0.8 mol, respectively. The suppression of dielectric constants is attributed to the absence of polar Si—OH and Si—H$_2$O functional groups and completion of hydrolysis in the hybrids. In HR2 hybrids, the reduction of dielectric constant is also ascribed to the addition of APTEOS which reduced the hydrophilicity of hybrids and thus limited the motions of polar functional groups. Calculation of porosity implied that the formation of silica xerogels in the hybrids is another plausible cause of dielectric constant decrement. However, the dielectric measurement in conjunction with TEM characterizations illustrated the growth control of orgSiO$_2$ to obtain a closed-form silica structure is the key issue to achieve the low-dielectric constant property in hybrids. Leakage current density measurement showed that the addition of orgSiO$_2$ nanoparticles in polymer matrix does not drastically affect the charge carrier transport in the hybrids. In comparison with the electrical data reported by

previous studies, the fluorinated PI–orgSi$O_2$ hybrid thin films prepared in this work possessed satisfactory electrical properties, e.g., relatively low dielectric constant and leakage current density. Promising applications of such hybrids as the ILD layers for IC fabrication and/or insulating materials for electronic packaging can thus be expected if further studies relating to device integration, e.g., mechanical properties, adhesion, planarization, etc. were completed.

## Acknowledgement

This work was supported by the National Science Council, Taiwan, ROC, under the contract No. NSC94-2216-E-009-026.

## References

[1] Wary J, Olson R, Beach W. Semicond Int 1996;19(6):211–6.
[2] Jin Y, Ajmera PK, Lee GS, Singh V. J Electronic Mater 2005;34(9):1193–2105.
[3] Kim SH, Moon HS, Woo SG, Ahn J. Jpn J Appl Phys Part I 1999;38(12B):7122–5.
[4] Aziz R, Beamish JC. Circuit World 1998;24(2):24–33.
[5] Huang J, Xiao Y, Mya KY, Liu X, He C, Dai J, et al. J Mater Chem 2004;14(19):2858–63.
[6] Stevens NSM, Rezac ME. Polym 1999;40(15):4289–98.
[7] Ahmad Z, Mark JE. Chem Mater 2001;13(10):3320–30.
[8] Kim Y, Kang E, Kwon YS, Cho WJ, Cho C, Chang M, et al. Synth Met 1997;85(1–3):1399–400.
[9] Ree M, Goh WH, Kim Y. Polym Bull 1995;35(1–2):215–22.
[10] Hedrick JL, Cha HJ, Miller RD, Yoon DY, Brown HR. Macromolecules 1997;30(26):8512–5.
[11] Kioul A, Mascia L. J Non-Cryst Solids 1994;175(2–3):169–86.
[12] van Bommel MJ, Bernards TNM, Boonstra AH. J Non-Cryst Solids 1991;128(3):231–42.
[13] Jang K, Kim H. J Sol–gel Sci Techn 2007;41(1):19–24.
[14] Duran A, Serna C, Fornes V, Navarro JMF. J Non-Cryst Solids 1986;82(1–3):69–77.
[15] Li WS, Shen ZX, Zheng JZ, Tang SH. Appl Spectrosc 1998;52(7):985–9.
[16] Atkins GR, Krolikowska RM, Samoc A. J Non-Cryst Solids 2000;265(3):210–20.
[17] Park HB, Lee YM. Adv Mater 2005;17(4):477–83.
[18] Olejniczak Z, Łęczka M, Cholewa-Kowalska K, Wojtach K, Rokita M, Mozgawa W. J Mol Struct 2005;744–747(1–3):465–71.
[19] Chiang CL, Ma CCM. Polym Degrad Stabil 2004;83(2):207–14.
[20] Barsbay M, Can HK, Güner A, Rzaev ZMO. Polym Adv Technol 2005;16(1):32–7.
[21] Zhang QG, Liu QL, Jiang ZY, Chen Y. J Membrane Sci 2007;287(2):237–45.
[22] Capadona LA, Meador MAB, Alunni A, Fabrizio EF, Vassilaras P, Leventis N. Polymer 2006;47(16):5754–61.
[23] Nandi M, Conklin JA. Chem Mater 1991;3(1):201–6.
[24] Liu WD, Zhu BK, Zhang J, Xu YY. Polym Adv Technol 2007;18(7):522–8.
[25] Zhang J, Zhu BK, Chu HJ, Xu YY. J Appl Polym Sci 2005;97(1):20–4.
[26] Yu S, Wong TKS, Hu X, Pita K. Thin Solid Films 2004;462–463(1–2):311–5.
[27] Hong JK, Kim HR, Park HH. Thin Solid Films 1998;332(1–2):449–54.
[28] Hrubesh LW, Keene LE, Latorre VR. J Mater Res 1993;8(7):1736–41.
[29] Jo MH, Hong JK, Park HH, Kum JJ, Hyun SH. Microelectron Eng 1997;33(1–4):343–8.
[30] Henning S, Svensson L. Phys Scripta 1981;23(4B):697–702.
[31] Yu S, Wong TKS, Hu X, Pita K. Thin Solid Films 2004;462–463:311–5.
[32] Garrou P, Turlik I. In: Messner G, Turlik I, Blade JW, Garrou PE, editors. Thin film multichip modulus. Reston, VA, USA: International Society of Hybrid Microelectronics; 1992. p. 93–155.
[33] Plawsky JL, Achanta R, Cho W, Rodriguez O, Saxena R, Gill WN. In: Baklanov M, Green M, Maex L, editors. Dielectric films for advanced microelectronics. West Sussex, England: John Wiley & Sons; 2007. p. 137–90.
[34] Lee YK, Murarka SP. J Mater Sci 1998;33(16):4105–9.
[35] Sugitani S, Matsuzaki H, Enoki T. Characteristics of low-k film deposited by plasma-enhanced CVD using a liquid BCB source. 2003 International Conf Compound Semiconductor Mfg. May 19-22, 2003. Scottsgale AZ, USA. Session 4-4.
[36] Chang TC, Tsai TM, Liu PT, Chen CW, Tseng TY. Thin Solid Films 2004;469–470:383–7.
[37] Liu PT, Chang TC, Yan ST, Li CH, Sze SM. J Electrochem Soc 2003;150(2):F7–F10.
[38] Chang TC, Liu PT, Tsai TM, Yeh FS, Tseng TY, Tsai MS, et al. Jpn J Appl Phys Part I 2001;40(5A):3143–6.
[39] Yin G, Ning Z, Yuan Q, Ye C, Xin Y. J Am Ceram Soc 2007;90(6):1943–5.
[40] Chang TC, Mor YS, Liu PT, Tsai TM, Chen CW, Sze SM, et al. Thin Solid Films 2001;398–399:637–40.
[41] Kim K, Kwon D, Lee DS. Thin Solid Films 1998;332:369–74.
[42] Lee MK, Shih CM, Chang SM, Wang HC, Huang JJ. Jpn J Appl Phys 2005;44(6):L220–3.
[43] Yu S, Wong TKS, Hu X, Goh TK. Thin Solid Films 2004;462–463:306–10.
[44] Jain A, Rogojevic S, Ponoth S, Agarwal N, Matthew I, Gill WN, et al. Thin Solid Films 2001;398–399:513–22.
[45] Yu S, Wong TKS, Hu X. J Sol–gel Sci Tech 2004;29(1):57–62.
[46] Lin Q, Cohen SA, Gignac L, Herbst B, Klaus D, Simonyi E, et al. J Polym Sci Part B Polym Phys 2007;45(12):1482–93.
[47] Jiang LY, Leu CM, Wei KH. Adv Mater 2003;14(6):426–9.